Field interference studies between bump magnets with different coil structures at Chinese Spallation Neutron Source

Y. Chen and J. Y. Tang*

Institute of High Energy Physics, CAS, Yuquan Road 19B, Beijing 100049, China

(Received 8 November 2007; published 13 March 2008)

For magnets arranged so closely that the distance between them is comparable to the magnet apertures, the field interference becomes important. This is the case in the injection region at the China Spallation Neutron Source (CSNS) where several bump magnets are used to create fixed and dynamic local orbit bumps for the beam injection using the H^- stripping and the phase space painting method. The reduction in the field integral due to the field interference will cause an orbit distortion, and the orbit bumps will be no longer localized. It is found that the end coil structure plays an important role in reducing the fringe field of a magnet. This has been analyzed by using both the image current method and three-dimensional magnetic field calculations. The saddle end coil instead of the compact end coil has been adopted at the CSNS. The relative reduction in the field integration after the optimization can meet the design requirement of about 1% or less.

DOI: 10.1103/PhysRevSTAB.11.032401 PACS numbers: 03.50.De, 41.85.Ar, 29.27.Ac, 85.70.−w

I. INTRODUCTION

In high intensity proton synchrotrons, the H^- stripping injection is the only method to accumulate a large number of particles in the ring. Both arc and straight sections can be used to host the injection system [1,2]. The injection in a dispersion-free straight section has the advantages such as: the transverse phase space painting is not affected by the ramping bending magnets; the ring properties are essentially not affected by the local orbit bumping; the upgrading of the injection system in future is more feasible. With this solution, the local orbit bump is created by a group of bump magnets to facilitate the arrangement of the other injection devices and the phase space painting will not be influenced by the ring lattice magnets. Because of very large acceptance required to alleviate the space-charge effects, the bump magnets have large apertures. The long extension fringe field of large aperture magnets and the tight arrangement will lead to the field interference that makes the local orbit bump expanded to the whole ring. Usually efforts should be paid to reduce the field interference.

The design goal of the China Spallation Neutron Source (CSNS) is to obtain the proton beam of 120/240 kW in two phases with a repetition rate of 25 Hz [3]. After the H^- beam is converted to the proton beam via stripping, the rapid cycling synchrotron accumulates and accelerates the proton beam from 80 MeV to 1.6 GeV. With the lattice design of fourfold symmetry, a zero-dispersion long drift of 9 m in length is used to accommodate the entire injection system (see Fig. 1), which contains a four-dipole chicane to form a horizontal orbit bump of 50 mm amplitude and eight symmetrically placed dynamic bump magnets for the phase space painting in both the horizontal and the vertical planes. The injection system is designed to accommodate both the correlated and the anticorrelated painting schemes [4–6].

II. FIELD INTERFERENCE BETWEEN CLOSE MAGNETS

When two magnets are installed closely, e.g., the distance between the iron yokes of the two magnets is comparable to the sum of the two magnet gaps, the fringe fields of the two magnets are overlapped. This is usually called the field interference [7–12]; it has many drawbacks and should be avoided or minimized. Unfortunately, the bump magnets in the CSNS injection region are in this situation. The main drawbacks of the field interference between the bump magnets are: the originally local orbit bump is expanded to the whole ring, thus the closed orbit distortion becomes worse; the painting process in the phase space is disturbed; the influence on the H^-/H^0 trajectories may lead to larger beam loss. Although the multipole components in the bump magnets of the window-frame type are important, to suppress them the bump magnets are paired in reverse field and powered in series; the contribution from the fringe field are negligible. Therefore, the influence on the multipole components due to the field interference is not considered here. As shown later, the main field interference between the bump magnets comes from the two adjacent horizontal painting bump (BH) and chicane bump (BC) magnets. The BC bump magnets are DC type and the BH magnets are dynamic with the magnetic field only during the injection period when the field interference in the injection region is important. The BC, BH, and vertical painting bump (BV) magnets are all powered in series to reduce the tracking errors, thus the field reductions in the BH and BC magnets cannot be compensated

*Corresponding author.
tangjy@ihep.ac.cn

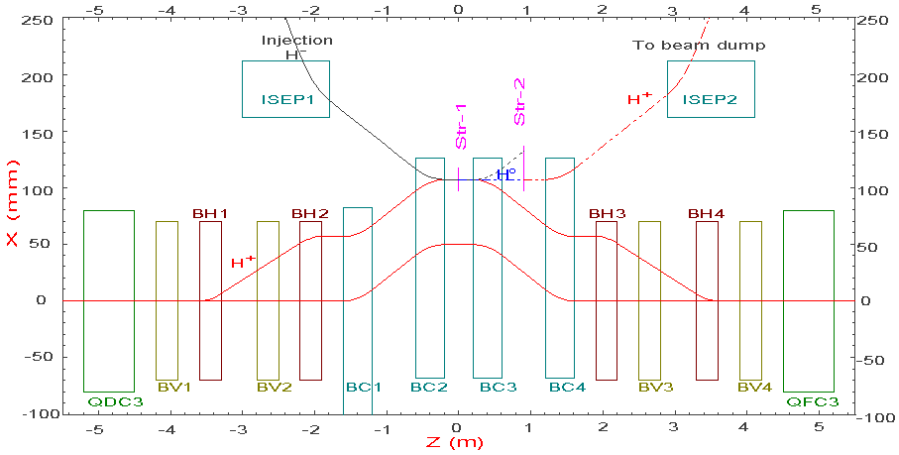

FIG. 1. (Color) Layout of the CSNS injection system. QDC3 and QFC3 stands for the ring quadrupoles, BC1-BC4 for the DC type bump magnets, BH1-BH4 for the horizontal painting bump magnets, BV1-BV4 for the vertical painting bump magnets, ISEP1-ISEP2 for the septum magnets, Str1-Str2 for the stripping foils.

and the influence to the closed orbit along the ring cannot be corrected by the correction dipoles that are much slower in the ramping rate. Taking into account the bump strengths of 50.0 mrad and 40.7 mrad for the BC and BH magnets, respectively, the requirement for the field reduction is set to about 1.0%, which results in a closed orbit distortion of about 3.6 mm at the maximum. On the side of the phase space painting, it is consistent to the tracking error requirement of less than 2%.

The field interference can be calculated using 3D magnetic field calculation codes. The code OPERA3D/TOSCA [13] has been used to calculate the field interference in the CSNS injection region. The main physical parameters of the bump magnets are given in Table I. Because the bump magnets are arranged symmetrically, the three bump magnets BC1, BH2, and BV2 as an entity are chosen for the field calculations. The preliminary magnet arrangement takes mainly into account the installation issue and the balance between the strength requirements to the magnets, and then the distances between the magnets are adjusted according to the field calculations. On the other hand, longer effective lengths for the magnets are helpful to reduce the excitation currents. The currents are very high (in the order of 10 000 A) with two-turn coils and difficult to produce. The calculation models for a group of three bump magnets are shown in Fig. 2. The bump magnets are designed to be compact with the end coil windings clinging to the iron yoke, which are similar to the ones used in other accelerators [14–16] and have the advantage of leaving more space for their installation.

TABLE I. Main parameters for the bump magnets.

Magnet	Gap height [cm]	Yoke length [cm]	Aperture width [cm]	Designed *BL* [Gauss cm]	Effective length [cm]
BV2	19. 0	19. 0	17. 0	39 635	30. 0
BH2	19. 4	18. 0	19. 4	37 740	30. 0
BC1	18. 0	29. 0	24. 6	65 884	40. 0

The distances between the magnets (BC1-BH2, BH2-BV2, in effective length) were initially set to 20 cm. The calculations using OPERA3D show that the field integral for BH2 is reduced by 4.75%, BC1 by 3.2%, and BV2 by

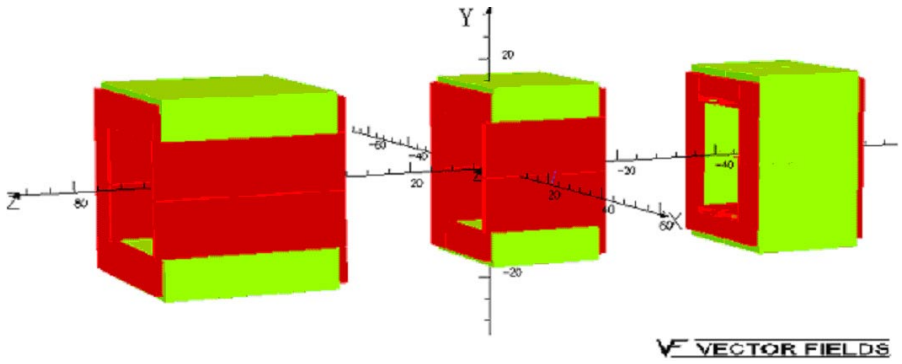

FIG. 2. (Color) Assembled model for the 3D field calculation of the bump magnets (compact end coil).

TABLE II. Comparison of the reductions in the field integral for the different distances between the two adjacent magnets.

Bump	With distance 20 cm (%)	With distance 30 cm (%)
BH2	4. 75	3. 14
BC1	3. 20	2. 05
BV2	0. 19	0. 17

0.19%. A field reduction here means the relative change by comparing the field integral including the field interference from an adjacent magnet with the one for the individual magnet. More details about the field interference are given in Sec. IV. This means that the field reduction is very important if the fields of the two adjacent magnets are in the same direction and almost negligible if they are in the orthogonal planes. For the given total length of the uninterrupted drift space, the distance between the magnets was enlarged from 20 to 30 cm, and better results are obtained, although the requirement of about 1% in the reduction of the field integral is still not met, see Table II. More efforts have been made to minimize the field interference, and this includes the use of a different end coil design to be discussed in the next sections.

III. INFLUENCE OF THE END COIL ON THE FRINGE FIELD

These kinds of bump magnets are usually designed to be a window-frame type for compactness. According to the superposition principle, the fringe field of a dipole magnet is composed of the field contributions by the horizontal current component, vertical current component, and the iron yoke. For the vertical component of the fringe field, the contributions are from the horizontal current component and the iron yoke, and this can be expressed by

$$B_y(z) = B_{y,x}(z) + B_{y,\mathrm{gap}}(z), \tag{1}$$

where $B_{y,x}$ is for the field produced by the current along the x-axis in the upper/lower end coil sections, $B_{y,\mathrm{gap}}$ is the field contribution produced by the main coil section and its magnetization in the yoke that is the main part of the fringe field. A larger magnet gap will have a longer extent for the $B_{y,\mathrm{gap}}$. The fringe field is evaluated along the beam or the z-axis (see Figs. 3 and 6). If the magnetic field in the yoke is not very high or the iron yoke is not saturated ($\mu_r \gg 1$), one can use the image current together with the end coil current to evaluate the contribution of the end coil to the fringe field [17].

Following the depiction in Fig. 3 and according to the Biot-Savart law, the vertical field component by the two current bars can be expressed:

$$B_{y,x} = -\frac{\mu_0 I}{4\pi}\left\{\int_{-w}^{w} \frac{z' - d/2}{(a^2 + l^2)^{3/2}}\,dl + \int_{-w}^{w} \frac{z' + d/2}{(b^2 + l^2)^{3/2}}\,dl\right\}, \tag{2}$$

where

$$a = \sqrt{\left(z' - \frac{d}{2}\right)^2 + h^2} \tag{3}$$

$$b = \sqrt{\left(z' + \frac{d}{2}\right)^2 + h^2}, \tag{4}$$

I is the current, a and b are the distances between the current or image current and the P, d is the distance between the current and the image current, z' is the distance between the iron end plane and the P, h is the height of the coil, w is the half-length of the coil section. The integrations in Eq. (2) can be simplified to

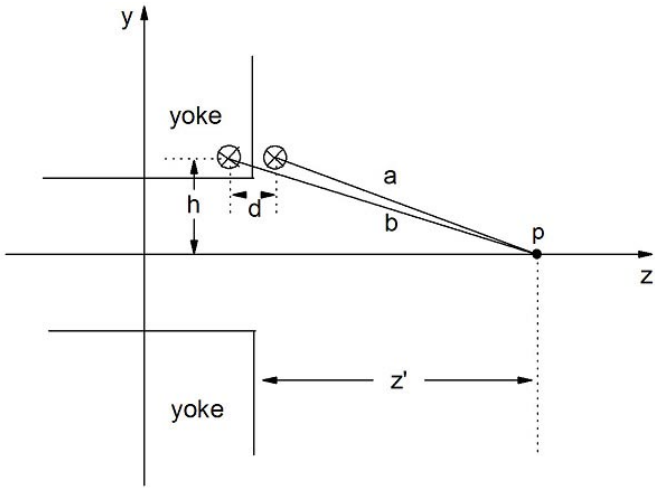

FIG. 3. Fringe field contribution by the end coil current using image current (the current is along the x-axis, pointing inward).

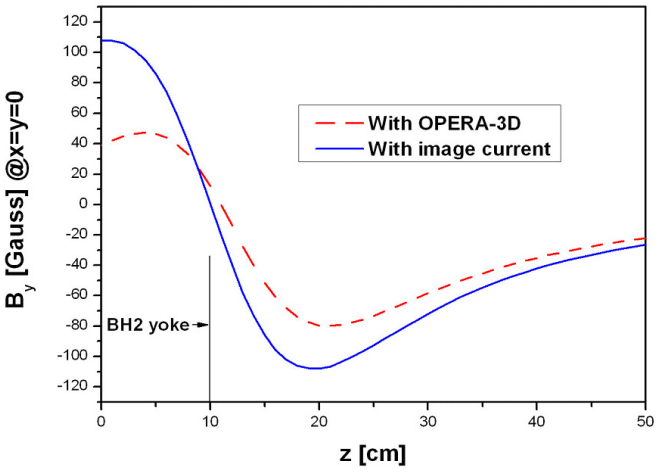

FIG. 4. (Color) Comparison of the end coils field between the image current method and the 3D numerical calculation method (valid for $z > z_0$, z_0 for the yoke end plane).

$$B_{y,x} = -\frac{\mu_0 I}{2\pi}\left\{\frac{w}{a^2\sqrt{a^2+w^2}}\left(z'-\frac{d}{2}\right) + \frac{w}{b^2\sqrt{b^2+w^2}}\left(z'+\frac{d}{2}\right)\right\}, \quad (\text{for } z' > 0). \quad (5)$$

To evaluate the method using the image current, the calculation result is compared with the one using OPERA3D where the magnet BH2 is taken only as an iron yoke, and shown in Fig. 4. They agree well on the distribution shape. The difference on the quantity, which is about 30% for the minimum value, is mainly due to the more complicated iron structure used in the OPERA3D calculations. This means that the end coil current is helpful to reduce the fringe field produced by the main coil section and its magnetization in the yoke. According to Eq. (5), the negative well is deeper when the coil is lower (smaller h), and this principle can be used to reduce the fringe field range. In the next section, different types of end coils will be compared based on this principle. Although the half-length of the end coil (w) has also an effect in the fringe field, it is almost determined by the global design of the magnet and will not be optimized to reduce the fringe field.

IV. FRINGE FIELD USING DIFFERENT END COIL STRUCTURES

As mentioned in Sec. III, the end coil of a bump magnet contributes significantly to the fringe field. This characteristic can be used to design different end coil shapes to reduce the fringe field. As suggested by Eq. (5), both lower coil height and smaller d value can help to reduce the fringe field. In order to evaluate the contributions of these two factors to the fringe field, direct calculations using Eq. (5) for the three different parameter settings are shown in Fig. 5. Although the shapes of the field contributions are somewhat different when changing the two parameters, Fig. 5 indicates clearly that it is more interesting to have

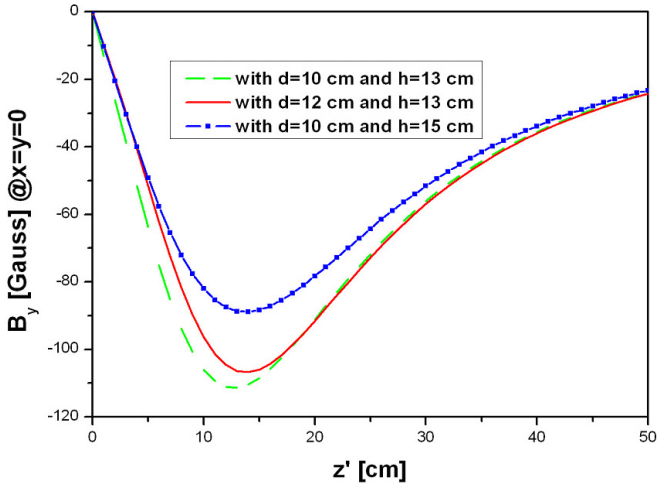

FIG. 5. (Color) Comparison of the field distributions with different current positions using the image current method.

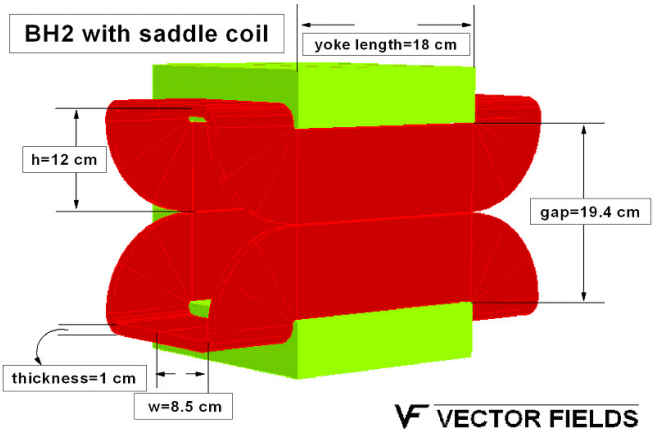

FIG. 6. (Color) Structure of the bump magnet BH2 with the saddle end coil.

smaller h to reduce the fringe field. This means the end coil pattern oriented horizontally is favored over the one oriented vertically. Thus, the saddle end coil type should be better than the compact end coil. Figure 6 shows the structure and the parameters of the bump magnet BH2. The numerical calculation results also indicate that the saddle end coil is favored over the compact coil for reducing the fringe field, which is consistent with the results by the image current method. The comparison of the field distributions between the two types of end coils for the bump magnet BC1 using OPERA3D is shown in Fig. 7. For the main part of the field distribution the saddle end coil is slightly better as the field distribution is closer to the hard-edge type. With the saddle end coil adopted for the CSNS, the model of the BC1-BH2-BV2 magnet group for the OPERA3D calculations is shown in Fig. 8. The field interference is also shown in Fig. 9 for the magnets BC1 and BH2, where the field calculations for the individual magnets are compared with the one for the grouped magnets. When the two fringe fields are overlapped, the reverse field

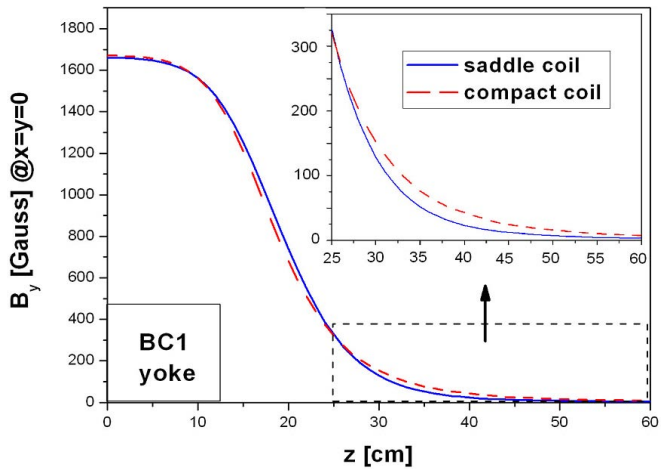

FIG. 7. (Color) Field comparison between the two different end coils for BC1 using 3D field calculations.

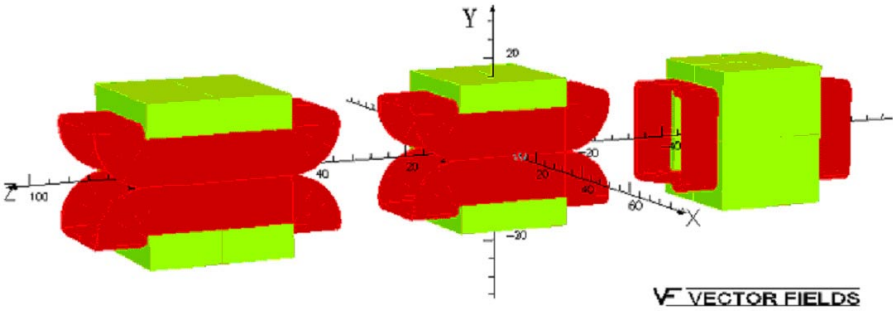

FIG. 8. (Color) Assembled model for the field calculation with the bump magnet group using the saddle end coil.

directions in the BC1 and BH2 will reduce both the field extension ranges. Both the new fringe fields stop at the zero-field crossing, thus the two field integrals are reduced. At the CSNS, the methods of choosing the special saddle end coil and increasing the distance between the bump magnets are used to reduce the field overlapping. It is found that the two orthogonal fields have almost no interference, and this can be seen in Fig. 10 and in Table III. In

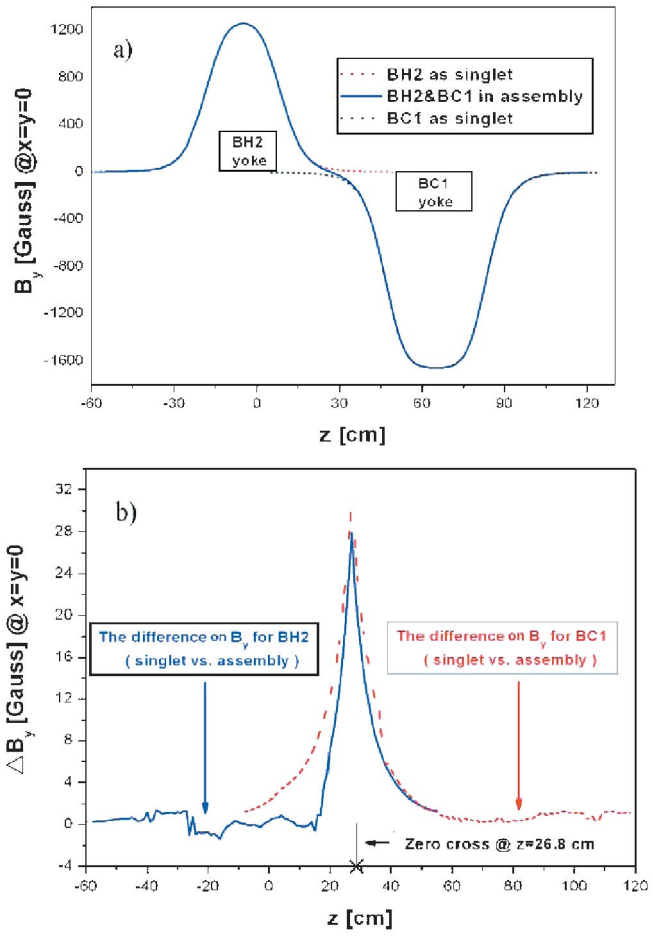

FIG. 9. (Color) Comparison between the field distributions (dashed lines) calculated for the individual magnets and the one (solid line) calculated for the grouped magnets (all with the saddle end coils). (a) Absolute field. (b) Field difference.

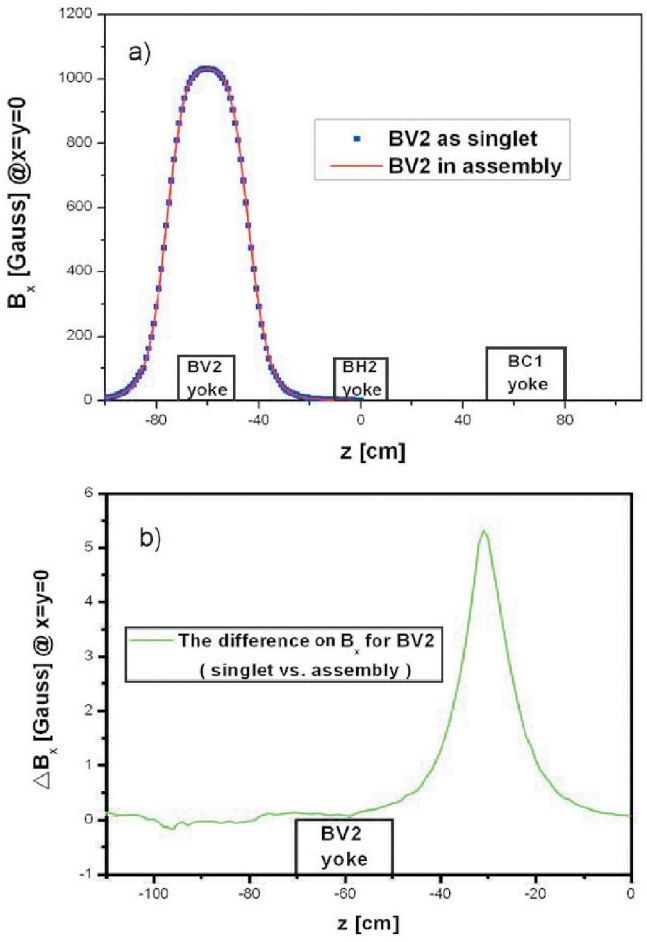

FIG. 10. (Color) Distribution of vertical field component in the grouped magnets using 3D field calculations. (a) Absolute field. (b) Field difference.

TABLE III. Comparison of the reduction in the field integrals for different end coil types.

Magnet	Compact coil (%)	Saddle coil (%)
BH2	3. 14	1. 10
BC1	2. 05	0. 80
BV2	0. 17	0. 14

this case, the adjacent magnet is just like an iron piece without current excitation.

With the saddle end coil design for all the bump magnets, the reductions in the field integrals due to the field interference are reduced to about 1% or even smaller (see Table III), and this meets the design requirements. The different reductions in the field integrals for the tied BC1 and BH2 magnets are due to the higher field and the larger effective length for the BC1.

Besides the relatively tight space for the installation of the magnets and the vacuum ducts as mentioned in Sec. II, there are other technical issues for the realization of the bump magnets using the saddle end coils. The fixing of the coils under the very strong magnetic force that is dynamic for the painting bump magnets BH1-BH4 and BV1-BV4 requires special attention. The inductance that is important for the painting bump magnets is almost the same for the two types of end coils. No critical technical problems concerning the saddle end coils have been found in the technical design of the BH prototype that is under fabrication, and no extra cost is needed in choosing the saddle end coil.

Comparing with the method using the saddle end coil that gives a satisfactory result in reducing the fringe field in the case of the CSNS without extra cost, one can also consider other methods such as field clamp and bucking current that are often more effective to reduce the fringe field. However, in the case of the fast-pulsed bump magnets as used in the CSNS injection, the eddy-current effect is very important so that the use of the field clamp method is disfavored. The bucking current method is also difficult to apply here due to the coil support problem and the high cost for the programmed power supply similar to the one for driving the main coil. If an ordinary dipole is considered, all the methods mentioned above may be considered to reduce the fringe field according to the application environment.

V. CONCLUSIONS

Through the analysis on the end coil contribution to the fringe field using both the image current and OPERA3D field calculation methods, it is found that the end coil of a window-frame-type magnet can play a very useful role in reducing the fringe field range. The image current method shows the relations between the parameters intuitively, and suggests the use of the end coil pattern oriented horizontally. Thus, the saddle end coil instead of the compact end coil is adopted for the bump magnets in the CSNS injection region. After the optimization on the magnet distances, the yoke lengths, and the end coils, the reductions in the field integrals of the bump magnets can be controlled to about 1% or less, which meet the design requirements. The end coil method should be applicable in the other cases where it is important to shorten the fringe field extension.

ACKNOWLEDGMENTS

This work was supported by the National Natural Science Foundation of China (10775153) and the CAS Knowledge Innovation Program-"CSNS R&D Studies". The authors would like to thank Dr. W. Z. Meng of BNL for help on the OPERA3D calculation skills, and W. Kang and the other CSNS colleagues for the discussions.

[1] J. Wei *et al.*, Proceedings of PAC 2001, Chicago, pp. 2560–2562.
[2] G. H. Rees, CERN Accelerator School, CERN 94-01, pp. 731–743.
[3] J. Wei *et al.*, Proceedings of APAC 2007, Indore, pp. 310–314, http://accelconf.web.cern.ch/AccelConf/.
[4] J. Y. Tang *et al.*, High Energy Phys. Nucl. Phys. **30**, 1184 (2006).
[5] J. Y. Tang *et al.*, Proceedings of EPAC 2006, Edinburgh, pp. 1783–1785, http://accelconf.web.cern.ch/AccelConf/.
[6] J. Qiu *et al.*, Proceedings of EPAC 2006, Edinburgh, pp. 1774–1776, http://accelconf.web.cern.ch/AccelConf/.
[7] Y. Papaphilippou *et al.*, Proceedings of PAC 2001, Chicago, pp. 1667–1669, http://accelconf.web.cern.ch/AccelConf/.
[8] J. G. Wang *et al.*, Proceedings of PAC 2005, Knoxville, pp. 3865–3867, http://accelconf.web.cern.ch/AccelConf/.
[9] M. Shirakata *et al.*, Proceedings of EPAC 2002, Paris, pp. 1670–1672, http://accelconf.web.cern.ch/AccelConf/.
[10] J. G. Wang, Phys. Rev. ST Accel. Beams **9**, 122401 (2006).
[11] A. Morita *et al.*, Phys. Rev. ST Accel. Beams **4**, 122401 (2001).
[12] M. Berz, B. Erdélyi, and K. Makino, Phys. Rev. ST Accel. Beams **3**, 124001 (2000).
[13] OPERA-3D (an operating environment for electromagnetic research and analysis) is the preprocessing and postprocessing system for electromagnetic analysis programs such as TOSCA (for nonlinear magnetostatic or electrostatic field and current flow problems) developed by Vector Fields Limited, England.
[14] C. Pai *et al.*, Proceedings of PAC 2003, pp. 2144–2146, http://accelconf.web.cern.ch/AccelConf/.
[15] T. Takayanagi *et al.*, Proceedings of PAC 2005, Knoxville, pp. 1048–1050, http://accelconf.web.cern.ch/AccelConf/.
[16] I. Sakai *et al.*, Proceedings of PAC 2003, pp. 1512–1514, http://accelconf.web.cern.ch/AccelConf/.
[17] J. D. Jackson, *Classical Electrodynamics—Third Edition* (John Wiley & Sons, Inc., Singapore, 1999), p. 229.